

The Canada-France High- z Quasar Survey: 1.2 mm Observations (Research Note)

Alain Omont^{1,2}, Chris J. Willott³, Alexandre Beelen⁴, Jacqueline Bergeron^{1,2}, Gustavo Orellana^{5,4}, and Philippe Delorme⁶

¹ UPMC Univ Paris 06, UMR7095, Institut d'Astrophysique de Paris, F-75014, Paris, France

² CNRS, UMR7095, Institut d'Astrophysique de Paris, F-75014, Paris, France

³ Herzberg Institute of Astrophysics, National Research Council, 5071 West Saanich Rd, Victoria, BC V9E 2E7, Canada

⁴ Univ Paris-Sud and CNRS, Institut d'Astrophysique Spatiale, UMR8617, Orsay, F-91405, France

⁵ Astronomy Department Universidad de Concepción, Concepción, Chile

⁶ UJF-Grenoble 1/CNRS-INSU, Institut de Planétologie et d'Astrophysique de Grenoble (IPAG) UMR 5274, 38041, Grenoble, France

November 14, 2017

ABSTRACT

We report 250 GHz (1.2 mm) observations of a sample of 20 QSOs at redshifts $5.8 < z < 6.5$ from the the Canada-France High- z Quasar Survey (CFHQS), using the Max-Planck Millimeter Bolometer (MAMBO) array at the IRAM 30-metre telescope. A rms sensitivity $\lesssim 0.6$ mJy was achieved for 65% of the sample, and $\lesssim 1.0$ mJy for 90%. Only one QSO, CFHQS J142952+544717, was robustly detected with $S_{250\text{GHz}} = 3.46 \pm 0.52$ mJy. This indicates that one of the most powerful known starbursts at $z \sim 6$ is associated with this radio loud QSO. On average, the other CFHQS QSOs, which have a mean optical magnitude fainter than previously studied SDSS samples of $z \sim 6$ QSOs, have a mean 1.2 mm flux density $\langle S_{250\text{GHz}} \rangle = 0.41 \pm 0.14$ mJy; such a $2.9\text{-}\sigma$ average detection is hardly meaningful. It would correspond to $\langle L_{\text{FIR}} \rangle \approx 0.94 \pm 0.32 10^{12} L_{\odot}$, and an average star formation rate of a few 100's M_{\odot}/yr , depending on the IMF and a possible AGN contribution to $\langle L_{\text{FIR}} \rangle$. This is consistent with previous findings of Wang et al. on the far-infrared emission of $z \sim 6$ QSOs and extends them toward optically fainter sources.

Key words. Galaxies: high-redshift – Galaxies: starburst – Galaxies: active – Infrared: galaxies – Submillimeter: galaxies

1. Introduction

The highest-redshift QSOs known, at $z \gtrsim 6$, are fascinating objects, providing crucial clues about the growth of supermassive black holes (SMBH), their host galaxies and their environment, when the Universe was less than 1 Gyr old, toward the end of the reionization epoch. Black holes of several $10^9 M_{\odot}$ were already in place (Willott et al. 2003, Kurk et al. 2007; Jiang et al. 2007; Mortlock et al. 2012). Such a rapid growth of the mass of early black holes puts extremely severe constraints on classical accretion Eddington limited by radiation pressure. It might point to the existence of a more efficient process for forming a massive black hole such as direct collapse without fragmenting (Begelman et al. 2006; Volonteri 2012).

In this context, it is obviously critical to accumulate more information about SMBH growth and the parallel formation of the first massive galaxies in the most massive dark matter halos at the reionization epoch. An important point to elucidate is to determine the black hole to galaxy mass ratio at this epoch, and to see how it compares to the current value at $z = 0$. A related piece of information is provided by the relationship between the galaxy growth by star formation and the QSO luminosity generated in black

hole accretion. Both processes mainly result from gas transport to the center of the galaxy. They should contribute in building the eventual tight relation between the masses of the black hole and the galaxy, even if this relation is mainly ruled by QSO feedback onto the interstellar gas.

As the emission of young stars is mostly channeled into the far-infrared (FIR) by dust in such massive starburst galaxies, the FIR luminosity, L_{FIR} , directly reflects the star formation rate (SFR). In the absence of multi-wavelength sampling of the FIR emission, one may assume a standard infrared spectral energy distribution (SED) (e.g. Wang et al. 2008), and thus directly derive L_{FIR} and SFR from measuring the continuum flux density at a single wavelength. At $z \gtrsim 6$, a single continuum observation in the $\lambda \sim 1$ mm window efficiently probes the bulk of the rest-frame FIR emission and provides thus a simple estimate of L_{FIR} and SFR. In addition, such ~ 1 mm observations yield valuable estimates of the dust mass in the host galaxy which reflects a combination of the gas mass and the metallicity.

After a series of such mm/submm studies of FIR properties of $z \sim 2\text{-}4$ QSOs (e.g. Omont et al. 2001; 2003; Carilli et al. 2001; Priddey et al. 2003), this method was successfully applied by Wang et al. (2008; 2011a) to investigate the FIR properties, inferred from 1.2 mm observations, of

40 $z \sim 6$ QSOs mainly discovered from the Sloan Digital Sky Survey (SDSS) (Fan et al. 2006). A significant fraction (30%) of Wang et al.'s $z \sim 6$ sample is detected at 1.2 mm, pointing to an excess of FIR emission dominated by a strong starburst with a star formation rate $\approx 500\text{-}1000 M_{\odot}/\text{yr}$. At the sensitivity of these studies, $\sim 1\text{-}1.5$ mJy at 1.2 mm, 70% of the QSOs are not detected, and for the whole sample the behavior of the FIR luminosity with respect to the bolometric luminosity L_{bol} is similar to that of all QSOs at any redshift, pointing to an important contribution of the AGN to the FIR emission.

Besides SDSS, the Canada-France High- z Quasar Survey (CFHQS) is the second largest provider of $z \sim 6$ QSOs. With 20 sources it accounts for about one third of the total number of QSOs at $5.7 < z < 6.5$. Coming from deeper optical surveys, the CFHQS sample contains QSOs optically much fainter than the main SDSS sample and also the SDSS deep southern survey. The purpose of this Note is to publish the results of the 1.2 mm survey of the 20 $z \sim 6$ CFHQS QSOs that we performed to extend the existing studies of FIR properties of QSOs at similar redshifts to optically fainter sources. For four of these sources, 1.2 mm results were already published in Willott et al. (2007). The exceptionally strong 1.2 mm flux density that we found for CFHQS J1429+5447, led to the selection of this source to search for CO(2-1) emission (Wang et al. 2011b). Together with those of Wang et al. (2011a), our results provide a useful background for the much deeper studies of submillimeter properties of optically faint $z \sim 6$ QSOs that we have already begun with The Atacama Large Millimeter/submillimeter Array (ALMA) (Willott et al. in prep.).

Cosmological parameters of $H_0 = 70 \text{ km s}^{-1} \text{ Mpc}^{-1}$, $\Omega_M = 0.28$ and $\Omega_{\Lambda} = 0.72$ (Komatsu et al. 2009) are assumed throughout.

2. Observations

The CFHQS is an optically-selected survey for $5.8 < z < 6.5$ QSOs. It was carried out in regions of the sky observed as part of the Canada-France-Hawaii Telescope Legacy Survey¹, the Subaru/XMM-Newton Deep Survey and the Red-sequence Cluster Survey 2. With z'_{AB} band magnitude survey limits ranging from $z'_{\text{AB}} = 22$ to $z'_{\text{AB}} = 24.5$ in different regions of the sky, CFHQS QSOs are typically 10 – 100 times lower luminosity than QSOs at the same redshift from the main SDSS sample (Fan et al. 2006) and many are less luminous than those from the SDSS Deep Stripe (Jiang et al. 2008; 2009). The CFHQS survey contains 20 spectroscopically-confirmed QSOs at $5.88 < z < 6.43$, a significant fraction of the total of ≈ 60 QSOs known at this epoch (Willott et al. 2007; 2009; 2010a,b). Table 1 contains the positions, redshifts, magnitudes, absolute magnitudes and bolometric luminosities of the full sample. Bolometric luminosities have been determined from the absolute magnitudes at 1450\AA assuming a bolometric conversion factor $\zeta_{1450\text{\AA}} = L_{\text{bol}}/(\nu L_{\nu,1450\text{\AA}})$ of 4.4 (Richards et al. 2006).

The millimeter observations were performed within the pool observing sessions at the IRAM 30m telescope in the winters 2007 through 2010, using the 117 element version of the Max Planck Millimeter Bolometer (MAMBO) array (Kreysa et al. 1998) operating at an average wavelength of

1.2 mm (250 GHz). We used the standard on-off photometry observing mode, chopping between the target and sky by $32''$ in azimuth at 2 Hz every 10 s, and nodding the telescope every 10 or 20 s (see e.g. Wang et al. 2011a). On average, the noise of the channel used for point-source observations was about $35\text{-}40 \text{ mJy} \cdot \sqrt{s} / \text{beam}$. This allowed us to achieve rms $\lesssim 0.5\text{-}1.0$ mJy for 18 of the 20 sources, with about 0.5-1.5 hr of telescope time per source. Unfortunately, poor weather conditions during the last observing runs prevented us to reach the aimed rms of ~ 0.6 mJy for 8 sources out of 20. The data were reduced with standard procedures to minimize the sky noise with the MOPSCIP package developed by Zylka (1998).

The results are shown in Table 1. Only the peculiar source CFHQS J1429+5447 is detected with a signal to noise ratio $S/N > 5$. Two other sources, CFHQS J0033-0125 (Willott et al. 2007) and CFHQS J0102-0218, are marginally detected with $S/N = 3.1$ and 2.7, respectively, thanks to special deeper observations bringing the rms below 0.4 mJy. There are 10 other sources with rms between 0.45 and 0.65 mJy, and five between 0.75 and 1.0 mJy, all with $S/N < 2$.

Such a 3σ detection rate of barely 10% is significantly smaller than that of Wang et al. (2011a) who report a rate of 30%. This difference may be partially due to our lower sensitivity - average rms 0.69 mJy instead of 0.52 mJy for Wang et al.'s sources with $m_{1450} > 20.2$. However, there is certainly also an effect of the larger bolometric luminosities of Wang et al.'s sample, as discussed in Sec. 4.

3. Far-infrared luminosities

3.1. Estimates of L_{FIR} and M_{dust}

One may convert the 250 GHz flux densities - corresponding to $\lambda_{\text{rest}} \sim 170 \mu\text{m}$ - to FIR luminosities by assuming a model for the FIR SED. For homogeneity, we take the same assumptions as Wang et al. (2008; 2011a) for this SED, i.e. assume an optically thin graybody with a dust temperature of $T_d = 47$ K and emissivity index of $\beta = 1.6$. As proposed by Beelen et al. (2006), these are typical values for the FIR luminous QSOs at $z \sim 2\text{-}4$. We also select the same wavelength range, $42.5 - 122.5 \mu\text{m}$, for the definition of the FIR luminosity as Wang et al. (2008; 2011a). Values of L_{FIR} thus calculated for detected or tentatively detected sources are reported in Table 2. For the average redshift of our sample, $\langle z \rangle = 6.09$, the conversion factor between the average values of the 250 GHz flux density and L_{FIR} is

$$\langle L_{\text{FIR}} \rangle / 10^{12} L_{\odot} = 2.30 \times \langle S_{250\text{GHz}} \rangle (mJy) \quad (1)$$

For other redshifts the conversion factor is slightly different, varying from 2.35 for $z = 5.88$ to 2.16 for $z = 6.43$.

However, we note that our faint sources have much lower mm fluxes than the typical sources used to determine the dust temperature value $T_d = 47$ K. If our sources instead have parameters closer to those of nearby luminous infrared galaxies (LIRGs, $10^{11} - 10^{12} L_{\odot}$, $T_d \approx 33$ K, U et al. 2012), then the values of L_{FIR} would be ~ 3 times lower for $T_d = 33$ K.

The dust mass M_{dust} at T_{dust} is related to the FIR luminosity by $M_{\text{dust}} = L_{\text{FIR}} / 4\pi \int \kappa_{\nu} B_{\nu} d\nu$, where B_{ν} is the Planck function and $\kappa_{\nu} = \kappa_0 (\nu/\nu_0)^{\beta}$ is the dust absorption

¹ <http://www.cfht.hawaii.edu/Science/CFHTLS>

Table 1. Optical data and results of 1.2 mm observations of full CFHQS sample

Name	RA	DEC	Redshift [†]	m ₁₄₅₀ [*]	M ₁₄₅₀ [#]	L _{bol} (10 ¹³ L _⊙)	S _{250GHz} (mJy)	z' _{AB}
CFHQS J003311–012524	00:33:11.40	–01:25:24.9	6.13	21.53	–24.91	0.94	1.13±0.36	22.41±0.08
CFHQS J005006+344522	00:50:06.67	+34:45:22.6	6.253	19.84	–26.65	4.67	0.69±0.76	20.47±0.03
CFHQS J005502+014618	00:55:02.91	+01:46:18.3	5.983	21.82	–24.55	0.68	0.43±0.46	22.19±0.06
CFHQS J010250–021809	01:02:50.64	–02:18:09.9	5.95	22.02	–24.34	0.56	1.01±0.38	22.30±0.08
CFHQS J013603+022605	01:36:03.17	+02:26:05.7	6.21	22.04	–24.43	0.61	1.18±0.97	22.10±0.09
CFHQS J021013–045620	02:10:13.19	–04:56:20.9	6.4323	22.25	–24.31	0.70	1.14±0.93	22.67±0.05
CFHQS J021627–045534	02:16:27.81	–04:55:34.1	6.01	24.15	–22.24	0.08	0.37±0.57	24.40±0.06
CFHQS J022122–080251	02:21:22.71	–08:02:51.5	6.161	21.98	–24.47	0.63	–1.48±1.36	22.63±0.05
CFHQS J022743–060530	02:27:43.29	–06:05:30.2	6.20	21.41	–25.05	1.08	–0.03±0.53	22.71±0.06
CFHQS J031649–134032	03:16:49.87	–13:40:32.2	5.99	21.72	–24.66	0.75	2.76±1.44	21.72±0.08
CFHQS J105928–090620	10:59:28.61	–09:06:20.4	5.92	20.75	–25.60	1.79	0.03±0.82	20.82±0.03
CFHQS J142952+544717	14:29:52.17	+54:47:17.6	6.1831	20.59	–25.88	2.31	3.46±0.52	21.45±0.03
CFHQS J150941–174926	15:09:41.78	–17:49:26.8	6.121	19.63	–26.80	5.41	0.91±0.47	20.26±0.02
CFHQS J164121+375520	16:41:21.64	+37:55:20.5	6.047	21.19	–25.21	1.25	0.25±0.47	21.31±0.04
CFHQS J210054–171522	21:00:54.62	–17:15:22.5	6.087	21.37	–25.05	1.08	0.29±0.59	22.35±0.09
CFHQS J222901+145709	22:29:01.65	+14:57:09.0	6.152	21.90	–24.55	0.68	0.82±0.80	22.03±0.05
CFHQS J224237+033421	22:42:37.55	+03:34:21.6	5.88	22.09	–24.25	0.51	0.72±0.61	21.93±0.04
CFHQS J231802–024634	23:18:02.80	–02:46:34.0	6.05	21.55	–24.85	0.90	0.54±0.56	21.66±0.05
CFHQS J232908–030158	23:29:08.28	–03:01:58.8	6.417	21.53	–25.02	1.05	0.06±0.50	21.76±0.05
CFHQS J232914–040324	23:29:14.46	–04:03:24.1	5.90	21.96	–24.39	0.58	–1.45±0.63	21.87±0.08

[†] Redshifts are from Willott et al. (2007;2009;2010a;2010b;in prep.); Wang et al. (2011b). Redshifts to 4 decimal places are from millimeter lines, those to 3 decimal places are from broad UV MgII lines and those to 2 decimal places are from Ly- α .

^{*} Apparent magnitude at rest-frame 1450 Å.

[#] Absolute magnitude at rest-frame 1450 Å. The values given here supersede previous published values of M₁₄₅₀. They were derived by fitting a typical QSO spectrum to the observed *J*-band magnitudes.

coefficient. Using $\kappa_0 = 18.75 \text{ cm}^2 \text{ g}^{-1}$ at 125 μm (Hildebrand 1983) as Wang et al. (2008; 2011a), yields

$$M_{\text{dust}}/10^8 M_{\odot} = 0.40 \times L_{\text{FIR}}/10^{12} L_{\odot}. \quad (2)$$

For $T_{\text{d}} = 33 \text{ K}$, the values of M_{dust} would be ~ 7 times larger than for $T_{\text{d}} = 47 \text{ K}$ for the same L_{FIR} (~ 2.4 times larger for the same $S_{250\text{GHz}}$).

3.2. Average FIR Luminosities

Considering the small number of 1.2 mm detections, we use the additional information provided by the averages derived from various stacking of the observed 1.2 mm flux densities. However, some care must be taken in carrying out such averages because of the inhomogeneity of our data. As the redshift range of our sample is small, it is simpler to perform all the averages on the 1.2 mm flux density, $S_{250\text{GHz}}$, and to infer the corresponding average of L_{FIR} by using the conversion factor of Eq. 1 for the average redshift 6.09. We may consider the following various averages of $S_{250\text{GHz}}$:

- a) Classical rms weighted averages with weights proportional to $1/\text{rms}^2$. However, this could give too much weight to the two sources with $\text{rms} < 0.4 \text{ mJy}$ whose integration time was anomalously long. It seems thus better to replace their rms by a typical value - median of the rms of the other sources (regularized rms).

- b) Plain, straight average of the nominal values of $S_{250\text{GHz}}$ with equal weights irrespectively of the rms. How-

ever, this does not take into account the difference in quality of these values. Therefore, we give in Table 2 the result of such a straight average with discarding two sources whose 250 GHz rms are peculiarly large.

- c) As there is clearly one exceptional source, CFHQS J1429+5447, which is more than three times stronger at 1.2 mm than all the others, and is radio loud (Sec. 3.3), one may prefer to exclude it, stacking only the 19 other sources with weights as in a).

- d) One might also exclude the two other tentative detections, stacking only 17 sources with weights as in a).

- e) & f) One may finally try to split the sample into two halves with respect to the UV luminosity to see whether the latter can have some visible effect on $\langle S_{250\text{GHz}} \rangle$.

In Table 2, we give the results corresponding to all these options. It is seen that the results of the first two do not significantly differ. As expected, dropping CFHQS J1429+5447 leads to a decrease of the average flux density, yielding $\langle S_{250\text{GHz}} \rangle = 0.41 \pm 0.14$ for the rms weighted average of the 19 other sources. This is probably the best average for the most representative sources of our sample. But at 2.9σ it is hardly meaningful. In addition small residual systematic errors in MAMBO results are not excluded at this level.

Note that the average of $\log(L_{\text{FIR}})$ (or $S_{250\text{GHz}}$) for groups e) and f) is found to be about the same despite the fact these groups are split by luminosity. This may appear surprising because one may expect to see a decrease of $\langle L_{\text{FIR}} \rangle$ with $\langle L_{\text{bol}} \rangle$ in line with the results of Wang et

Table 2. Average properties

Group	Number	$\langle L_{\text{bol}} \rangle^{*av}$ ($10^{13} L_{\odot}$)	$\langle L_{\text{bol}} \rangle^{*med}$ ($10^{13} L_{\odot}$)	$\langle S_{250\text{GHz}} \rangle^{\dagger}$ (mJy)	$\langle L_{\text{FIR}} \rangle^{\ddagger}$ ($10^{12} L_{\odot}$)	$\langle M_{\text{dust}} \rangle^{\ddagger\ddagger}$ ($10^8 M_{\odot}$)
a) all objects	20	1.31	0.90	0.63 ± 0.14	1.45 ± 0.32	0.58
b) homogeneous	18	1.38	0.94	0.64	1.46	0.59
c) regular	19	1.26	0.75	0.41 ± 0.14	0.94 ± 0.32	0.38
d) 250 GHz-undetected	17	1.32	0.75	0.34 ± 0.15	0.78 ± 0.34	0.31
e) regular $m_{1450} < 21.7$	9	2.02	1.08	0.42 ± 0.19	0.96 ± 0.44	0.39
f) regular $m_{1450} > 21.7$	10	0.58	0.63	0.41 ± 0.22	0.94 ± 0.51	0.38
CFHQS J1429+5447 [#]	1	2.31		3.46 ± 0.52	7.85 ± 1.18	3.16
CFHQS J0033-0125	1	0.94		1.13 ± 0.36	2.58 ± 0.82	1.04
CFHQS J0102-0218	1	0.56		1.01 ± 0.38	2.35 ± 0.89	0.95

*: Bolometric luminosity: ^{av} mean value (straight average, with equal weight for all sources); ^{med} median value

†: Averages of $S_{250\text{GHz}}$ are performed as described in Sec. 3.2: groups a to f:

a): Whole sample, regularized rms weighted average.

b): All objects but CFHQS J0221–802 and CFHQS J0316–1340 whose 250 GHz rms are peculiarly large; straight average (with equal weight for all sources).

c): All objects but CFHQS J1429+5447 which is exceptionally strong at 250 GHz and radio loud (Sec. 3.2); regularized rms.

d): All objects but CFHQS J0033-0125, CFHQS J0102-0218 and CFHQS J1429+5447 which are (tentatively) detected; regularized rms.

e): Same as c), but $m_{1450} < 21.7$.

f): Same as c), but $m_{1450} > 21.7$.

[#]: The value used for L_{FIR} of CFHQS J1429+5447 corresponds to the totality of the measured 250 GHz flux density, while only an unknown part is emitted by the starburst dust in the QSO host galaxy.

††: $\langle L_{\text{FIR}} \rangle$ is inferred from $\langle S_{250\text{GHz}} \rangle$ through Eq. 1 (for all groups with several sources, the average redshift $\langle z \rangle = 6.09$ is assumed); $\langle M_{\text{dust}} \rangle$ is inferred from $\langle L_{\text{FIR}} \rangle$ through Eq. 2.

al. (2011a) (see lower dotted line in Fig. 1). However this can be easily explained by the fact we do not have a huge luminosity range in our sample. The average $\langle L_{\text{bol}} \rangle$ of these groups differ by a factor of 4 and the medians less than a factor of 2. Given each stack is detected at only $S/N \sim 2$, our results are consistent with the relation of Wang et al.

3.3. CFHQS J142952.17+544717.6

This QSO is the only one detected at 1.2 mm with a high S/N ratio, $S_{250\text{GHz}} = 3.46 \pm 0.52$ mJy. The corresponding values of the FIR luminosity and the dust mass are reported in Table 2. Besides being one of the mm-brightest $z \sim 6$ QSOs and one of the UV most luminous of our sample, it is remarkable in many respects. It is one of the only four known radio-loud $z \sim 6$ QSOs (see e.g. Frey et al. 2011) and has the highest redshift and strongest radio emission among them. The EVLA observation of its CO(2-1) line (Wang et al. 2011b), prompted by our 1.2 mm result, has shown a strong CO emission resolved in two peaks, one on top of the QSO position and the other 1.2'' away. Each corresponds to a gas mass larger than $10^{10} M_{\odot}$. The value of the ratio of the FIR to CO luminosities, $L_{\text{FIR}}/L'_{\text{CO}} = 300$, is just below the average of this ratio for the $z \sim 6$ QSOs where Wang et al. (2010) have detected CO. This indicates that probably most of the 1.2 mm continuum emission comes from dust and not from the radio source. The latter is compact and has a very steep radio spectrum (3.03 ± 0.005 , 0.99 ± 0.006 and 0.257 ± 0.015 mJy at 1.6, 5 and 32 GHz, respectively; Frey et al. 2011; Wang et al. 2011b). This is another indication that most of the millimeter emission

is due to dust, although a significant synchrotron contribution cannot be fully excluded. Moreover, it is not yet known how the observed 250 GHz flux density is shared between the dust emission of each galaxy, and possibly the synchrotron emission of the QSO. Therefore in Table 2 and Fig. 1, the value of L_{FIR} corresponds to the totality of the measured 250 GHz flux density, while only an unknown part is emitted by the starburst dust in the QSO host galaxy.

4. Discussion and conclusions

The most natural explanation for an excess of FIR emission is star formation. If the FIR emission is powered by a dusty starburst, there is a direct relation between SFR and L_{FIR} . The most generally used relation is given by Kennicutt (1998), $\text{SFR}(M_{\odot}/\text{yr}) = 1.72 \times 10^{-10} L_{\text{FIR}}(L_{\odot})$ for a Salpeter IMF and $8 < \lambda < 1000 \mu\text{m}$. However, the exact conversion factor significantly depends on the IMF and the selected wavelength range for estimating L_{FIR} . With our selected wavelength range, 42.5–122.5 μm , it is conservative to assume that $\text{SFR}(M_{\odot}/\text{yr}) \gtrsim 1.5 \times 10^{-10} L_{\text{FIR}}(L_{\odot})$.

For sources with large FIR excess, such as CFHQS J1429+5447, it is generally agreed that most of the FIR emission is powered by a starburst (see e.g. Beelen et al. 2006; Wang et al. 2008; Mor et al. 2012). This yields $\text{SFR} \gtrsim 500 M_{\odot}/\text{yr}$ for each of the two galaxies of CFHQS J1429+5447. For the other sources, making the assumption that all the FIR emission is due to star formation, the value of Table 2 (group c), $\langle L_{\text{FIR}} \rangle \approx 0.94 \pm 0.32 \times 10^{12} L_{\odot}$, would imply $\text{SFR} \gtrsim 140 \pm 50 M_{\odot}/\text{yr}$.

For the much smaller FIR emission of the majority of QSOs, an important starburst contribution is also likely;

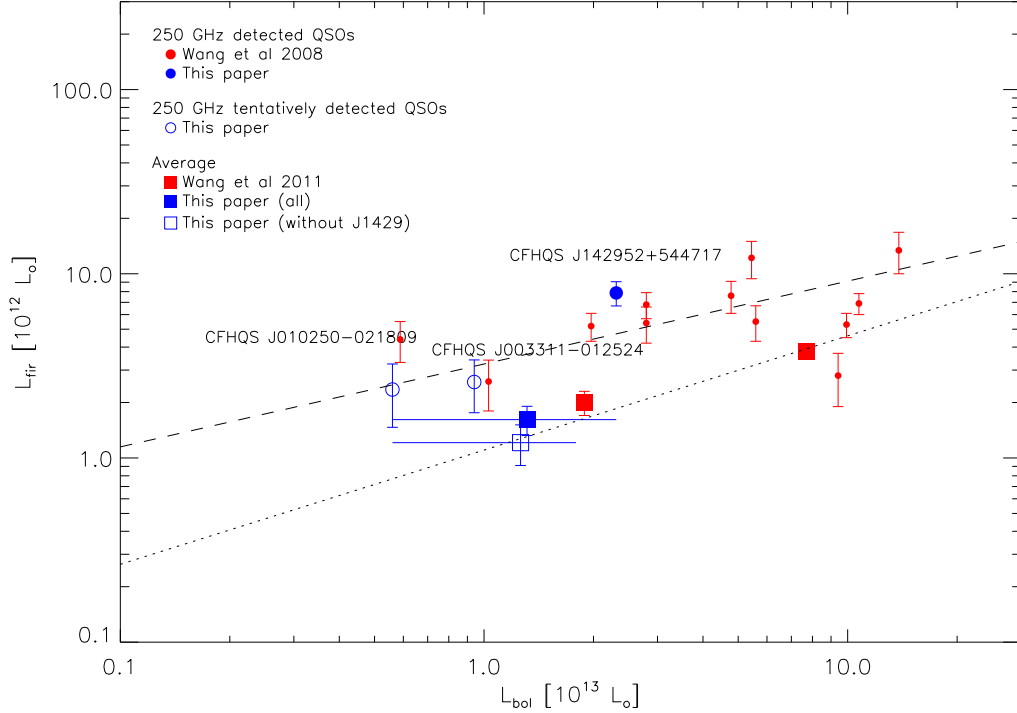


Fig. 1. Similar to Fig. 4 of Wang et al. (2011a). FIR and bolometric luminosity correlations of $z \sim 6$ QSOs, showing: 1) average luminosities (*large symbols*) for: 1a) our whole sample of 20 sources and that of 19 sources taking out CFHQ J1429+5447 (the horizontal error bars contain 80% of the data points of these samples, excluding the two highest and lowest values of L_{bol}); 1b) average values of Wang et al. (2011a) for optically faint ($m_{1450} \geq 20.2$) and bright ($m_{1450} < 20.2$) sources; 2) individual luminosities (*small symbols*) for our 250 GHz detections and tentative detections, together with the detections of Wang et al. (2008) for comparison. Note that for CFHQ J1429+5447, the value used for L_{FIR} corresponds to the totality of the measured 250 GHz flux density, while only an unknown part is emitted by the starburst dust in the QSO host galaxy. The two straight lines are reproduced from Fig. 4 of Wang et al. (2011a): The dotted line [$\log(L_{\text{FIR}}) = 0.62 \log(L_{\text{bol}}) + 3.9$] is a power-law fit to the average luminosities of all the QSO high- z samples, and the dashed line [$\log(L_{\text{FIR}}) = 0.45 \log(L_{\text{bol}}) + 6.6$] shows the power-law fit to the submillimeter or millimeter detected QSOs in all high- z samples and local ULIRGs. To be consistent with our selected bolometric conversion factor $\zeta_{1450A} = 4.4$ (Sec. 2), we have scaled all Wang et al.'s values of L_{bol} using our bolometric conversion factor instead of $\zeta_{1450A} \approx 6$ which we inferred from Table 4 and Fig. 4 of Wang et al. (2011a).

however, it is possible that a fraction also comes from dust powered by the AGN. This was pointed out for $z \sim 6$ QSOs by Wang et al. (2011a). They extended their discussion to lower redshifts as well as various authors that they quote (see also e.g. Rosario et al. 2012; Dai et al. 2012, for more recent references). In their Fig. 4, (partially reproduced in Fig. 1), they have shown that there is a remarkably uniform correlation of L_{FIR} with L_{bol} for QSO average luminosities, both for various samples of high- z QSOs, and of low- z ones (e.g. Hao et al. 2005). This correlation is well represented by the power law [$\log(L_{\text{FIR}}) = 0.62 \times \log(L_{\text{bol}}) + 3.9$] (see Fig. 1). A starburst contribution is needed to explain the FIR slope of 0.6, while the slopes for IRAS 12 μm and 25 μm of local QSOs are linear and consistent with AGN heating (Hao et al. 2005). However, such a relatively high value of 0.6 for the FIR slope may be evidence for a combination of AGN and starburst contributions.

In Fig. 1, similar to Fig. 4 of Wang et al. (2011a), we show the correlations for our sample between L_{FIR} and L_{bol} , computed as described above (Sec. 2). Comparing the plotted average luminosities for all our 20 sources, with and without CFHQ J1429+5447, to the averages of Wang et al. (2011a) for $m_{1450} < 20.2$ and > 20.2 , shows that our sam-

ple represents a significant extension to the work of Wang et al. toward optically weaker sources. Our average for all 20 observed sources, including CFHQ J1429+5447, appears consistent with the two averages of Wang et al. for all the $z \sim 6$ QSOs they observed, respectively optically faint and bright. The average for our 19 sources, without CFHQ J1429+5447, is in better agreement with the power-law fit that Wang et al. found for the average luminosities of all the high- z samples of QSOs observed in sub/millimeter.

The position of CFHQ J1429+5447 in Fig. 1 is well within the region of 1.2 mm detected sources by Wang et al. (2008; 2011a). Finally in Fig. 1 we have added the positions of the two tentatively detected sources at 1.2 mm, CFHQ J0033-0125 (S/N=3.1) and CFHQ J010250-0218 (S/N=2.7). They are again close to the line fitting mm-detected sources.

In conclusion, our 1.2 mm observations confirm the results of Wang et al. (2011) about the FIR emission of $z \sim 6$ QSOs and extend them toward optically fainter sources. The core of our sample is made of such faint sources, $21.5 \lesssim z'_{\text{AB}} \lesssim 22.7$, corresponding to $L_{\text{bol}} \sim (0.5-1) \times 10^{13} L_{\odot}$ and black-hole masses of a few $10^8 M_{\odot}$ (Willott et al. 2010b). For such QSOs, the average FIR luminosity

is weak, but probably still significant $\langle L_{\text{FIR}} \rangle \approx 0.94 \pm 0.32 \times 10^{12} L_{\odot}$. This corresponds to an average star formation rate of a few 100's M_{\odot}/yr . However, there is certainly a large dispersion for individual sources around these average values - at least a factor ~ 3 in both directions, as exemplified by our two tentative 1.2 mm detections (CFHQS J0033-0125 and CFHQS J0102-0218) in this L_{bol} range, and the very low 1.2 mm flux density measured with ALMA for two CFHQS QSOs (Willott et al. in prep.).

Such low star formation rates are probably reflecting small gas and total masses of the host galaxy. This should then favor large ratios $M_{\text{BH}}/M_{\text{galaxy}}$, which could be significantly larger than the typical ratio at $z = 0$ ($M_{\text{BH}}/M_{\text{bulge}} \approx 0.0014$; Marconi & Hunt 2003). But such ratios remain very uncertain in the absence of direct measurements of M_{gas} and M_{galaxy} , e.g. by CO or C^+ observations (e.g. Wang et al. 2011b; 2012; Willott et al. in prep.).

Acknowledgements. We thank T. Forveille for useful discussions. Based on observations with the IRAM 30m MRT at Pico Veleta. IRAM is supported by INSU/CNRS (France), MPG(Germany) and IGN(Spain). Thanks to the queue observers at IRAM who obtained data for this paper. Thanks to INSU for supporting a visit to France of G. Orellana. Based on observations obtained with MegaPrime/MegaCam, a joint project of CFHT and CEA/DAPNIA, at the Canada-France-Hawaii Telescope (CFHT) which is operated by the National Research Council (NRC) of Canada, the Institut National des Sciences de l'Univers of the Centre National de la Recherche Scientifique (CNRS) of France, and the University of Hawaii. This work is based in part on data products produced at TERAPIX and the Canadian Astronomy Data Centre as part of the Canada-France-Hawaii Telescope Legacy Survey, a collaborative project of NRC and CNRS.

References

- [1] Beelen, A., Cox, P., Benford, D. J., et al. 2006, ApJ, 642, 694
- [2] Begelman, M. C., Volonteri, M., & Rees, M. J. 2006, MNRAS, 370, 289
- [3] Carilli, C. L., Bertoldi, F., Rupen, M. P., et al. 2001, ApJ, 555, 625
- [4] Dai, Y., Bergeron, J., Elvis, M., et al. 2012, ApJ, 753, 33
- [5] Fan, X., Strauss, M. A., Becker, R. H., et al. 2006, AJ, 132, 117
- [6] Frey, S., Paragi, Z., Gurvits, L. I., Gabányi, K. É., & Cseh, D. 2011, A&A, 531, L5
- [7] Hao, C. N., Xia, X. Y., Mao, S., Wu, H., & Deng, Z. G. 2005, ApJ, 625, 78
- [8] Hildebrand, R. H. 1983, QJRAS, 24, 267
- [9] Jiang, L., Fan, X., Vestergaard, M., et al. 2007, AJ, 134, 1150
- [10] Jiang, L., Fan, X., Bian, F., et al. 2008, AJ, 135, 1057
- [11] Jiang, L., Fan, X., Annis, J., et al. 2009, AJ, 138, 305
- [12] Kennicutt, R. C., Jr. 1998, ARA&A, 36, 189
- [13] Komatsu, E., Dunkley, J., Nolta, M. R., et al. 2009, ApJS, 180, 330
- [14] Kreysa, E., Gemuend, H.-P., Gromke, J., et al. 1998, Proc. SPIE, 3357, 319
- [15] Kurk, J. D., Walter, F., Fan, X., et al. 2007, ApJ, 669, 32
- [16] Marconi, A., & Hunt, L. K. 2003, ApJ, 589, L21
- [17] Mor, R., Netzer, H., Trakhtenbrot, B., Shemmer, O., & Lira, P. 2012, ApJ, 749, L25
- [18] Mortlock, D. J., Warren, S. J., Venemans, B. P., et al. 2011, Nature, 474, 616
- [19] Omont, A., Cox, P., Bertoldi, F., et al. 2001, A&A, 374, 371
- [20] Omont, A., Beelen, A., Bertoldi, F., et al. 2003, A&A, 398, 857
- [21] Priddey, R. S., Isaak, K. G., McMahon, R. G., & Omont, A. 2003, MNRAS, 339, 1183
- [22] Richards, G. T., Lacy, M., Storrie-Lombardi, L. J., et al. 2006, ApJS, 166, 470
- [23] Rosario, D. J., Santini, P., Lutz, D., et al. 2012, A&A, 545, A45
- [24] U, V., Sanders, D. B., Mazzarella, J. M., et al. 2012, ApJS, 203, 9
- [25] Volonteri, M. 2012, Science, 337, 544
- [26] Wang, R., Wagg, J., Carilli, C. L., et al. 2008, AJ, 135, 1201
- [27] Wang, R., Carilli, C. L., Neri, R., et al. 2010, ApJ, 714, 699
- [28] Wang, R., Wagg, J., Carilli, C. L., et al. 2011a, AJ, 142, 101
- [29] Wang, R., Wagg, J., Carilli, C. L., et al. 2011b, ApJ, 739, L34
- [30] Wang, R., Wagg, J., Carilli, C. L., et al. 2012, arXiv:1210.0242
- [31] Willott, C. J., McLure, R. J., & Jarvis, M. J. 2003, ApJ, 587, L15
- [32] Willott, C. J., Delorme, P., Omont, A., et al. 2007, AJ, 134, 2435
- [33] Willott, C. J., Delorme, P., Reylé, C., et al. 2009, AJ, 137, 3541
- [34] Willott, C. J., Delorme, P., Reylé, C., et al. 2010a, AJ, 139, 906
- [35] Willott, C. J., Albert, L., Arzoumanian, D., et al. 2010b, AJ, 140, 546
- [Zylka 1998] Zylka, R. 1998, MOPSI Users Manual (Grenoble: IRAM)